Multi-platform Observations of Severe Typhoon Koinu

J. Y. He[1], P. W. Chan[2]*, C. W. Choy[2], P. Cheung[2], Y. W. Chan[2], C. C. Lam[2], Y. H. He[2], P. Rong[3], H. Su[3], and Z. M. Li[4,5]

[1]City University of Hong Kong, Kowloon Tong, Hong Kong.

[2]Hong Kong Observatory, Kowloon, Hong Kong.

[3]Dept. of Civil and Environmental Engineering, The Hong Kong University of Science and Technology, Clear Water Bay, Hong Kong

[4]Foshan Tornado Research Center, Foshan, Guangdong, China.

[5]China Meteorological Administration Tornado Key Laboratory, Foshan, Guangdong, China.

*Corresponding author: P. W. Chan (pwchan@hko.gov.hk)

Key Points:

- Observations from meteorological aircraft, ocean radar, and synthetic aperture radar show the structure of Severe Typhoon Koinu.
- Weather radar observations suggest the occurrence of a waterspout in the vicinity of Koinu.
- AI-based Pangu-Weather model outperforms the conventional global numerical weather prediction models in forecasting Koinu.

Abstract

Severe Typhoon Koinu passed south of Hong Kong on 8 and 9 October 2023, triggering the issurance of the Increasing Gale or Storm Signal No. 9, the second highest tropical cyclone warning signal in Hong Kong. Koinu was a difficult case for TC warning service due to its compact size and rather erratic movement over coastal waters of Guangdong. To monitor Koinu's movement and wind structure, the Hong Kong Observatory utilized various observational platforms, including meteorological aircraft, ocean radar, and synthetic aperture radar on polar orbiting satellites. The paper presents major observations derived from these measurements. The aircraft probe and drosonde data suggested boundary layer inflow, warm core structure, eyewall updraft and downdraft, and high turbulence in the eyewall of the typhoon. The weather radar observations indicated occurrence of a waterspout in the vicinity of the typhoon. Additionally, the study evaluates the forecasting performance of the AI-based Pangu-Weather model, and the results highlight its better performance than the global numerical weather prediction models in forecasting tropical cyclones in the region. The documentation of these observations aims to provide valuable references for weather forecasters and stimulate further research on forecasting this type of tropical cyclones.

1 Introduction

September and October 2023 were eventful months for the occurrence of weather-related natural hazards over southern China. In early September, the region was affected by Super Typhoon Saola which was a rather small tropical cyclone (TC) yet the second most intense TC affecting the South China Sea since 1950. From the radar pictures of Hong Kong when Saola got close to the territory, the eyewall had a diameter of around 70 km only. Saola's eye further shrank in size when it passed south of Hong Kong. It is a rather special cyclone bringing hurricane force winds to Hong Kong and the case has been documented in a number of papers, including observational study (Chan et al., 2023a), aircraft data (He et al., 2023), and forecast (Chan et al., 2023b). About a week later, the remnant of TC Haikui brought torrential rain to the Pearl River Estuary and its neighbouring areas. The Hong Kong Observatory (HKO) registered a record-breaking hourly rainfall of 158.1 millimetres ending midnight on 7 September 2023 since records began in 1884. It led to serious flooding at a number of places in Hong Kong.

On the evening of 8 October 2023, Severe Typhoon Koinu, surprisingly took on a northerly track towards Hong Kong for a few hours when it was located to the coastal waters south of the territory. In view of public safety, the Increasing Gale or Storm Signal No. 9 in Hong Kong was issued for the second time of the year. Koinu was even more compact than Saola. From the radar pictures of Hong Kong, its eyewall had a diameter of around 50 km only. However, when being affected by the outer periphery of the eyewall of Koinu, a weather station at around 40 km south of Hong Kong, namely, Huangmao Zhou (HMZ), had registered the wind rising from around 40-50 knots to over 90 knots within an hour only. Winds at HMZ continued to increase afterwards, reaching a peak of around 110 knots. Because of the relatively small size, Koinu was generally poorly captured by the global numerical weather prediction models with a horizontal resolution of the order of 10 km only.

To monitor the movement and changes in the wind structure of Koinu, the HKO made use of a variety of measurement platforms, including meteorological aircraft, the newly installed ocean radar, and the newly available synthetic aperture radar (SAR) onboard polar orbiting satellites in real time. This paper summarizes the major observations from these measurements. A waterspout was suspected to occur in the vicinity of the territory in association with Koinu, and observations of which are also included in this paper. Finally there would be a short section on the forecasting aspect of Koinu. It turned out the AI-based Pangu-Weather (Bi et al., 2023) forecasts using deep-learning techniques with different sets of model initial field were capable of forecasting the proximity of Koinu to Hong Kong about 5 days ahead, and as such in medium term (3 to 5 days) the performance of Pangu-based models was generally better than that of the conventional global numerical weather prediction models, which has also been reported for the case of Saola (Chan et al., 2023b). It is hoped that the documented materials would be useful for reference by weather forecasters in the future, and could stimulate further study on forecasting this type of rather special TC in autumn in the northern part of the South China Sea.

2 Life history of Koinu

Koinu formed as a tropical depression over the western North Pacific to the east of the Philippines on 29 September 2023. It started to move northwestwards towards the seas east of

Taiwan and intensified gradually in the next four days. Koinu intensified into a severe typhoon and reached its peak intensity on 2 October 2023 with a maximum sustained wind of 95 knots near its centre. Koinu turned to move west-southwestwards on 4 October 2023 and weakened into a typhoon after skirting past the southern tip of Taiwan on 5 October 2023. While satellite picture depicted the shrinking of Koinu's circulation, it unexpectedly intensified again into a severe typhoon on 7 October around 200 km southeast of Hong Kong with a maximum sustained wind of 95 knots. Koinu started to drift slowly northwestwards on the afternoon of 7 October 2023 and it even took a more northerly track towards Hong Kong on the afternoon of 8 October 2023. Koinu came closest to Hong Kong on the night of 8 October 2023 with its centre passing only about 70 km south of the Hong Kong Observatory. It started to move west to west-southwestwards across the western coast of Guangdong afterwards and finally degenerated into an area of low pressure on the night of 9 October 2023.

3 Aircraft observations

Three aircraft reconnaissance flights had been conducted for Koinu, namely the morning and evening of 6 October, and the morning of 7 October. Air data probe had collected useful data for these three flights. In particular, for the flight of 7 October, the aircraft was involved in a search and rescue exercise and low level flights had been conducted. For the two flights of 6 October, dropsondes had been released near the centre of Koinu.

The probe data was collected by the Aircraft Integrated Meteorological Measuring System 20 Hz (AIMMS20), and the descriptions of the system can be found in Beswick et al. (2008) and Chan et al. (2011). The plots of wind data from the aircraft data probe for the three flights are shown in Figure 2. In the first flight, winds were found to be lighter within the eyes and hurricane force winds were found just around the eyewall (Figure 2(a)). In the second flight, the flight pattern was more complex and there was not a clear pattern about the distribution of the winds (Figure 2(b)). Hurricane force winds were found at a limited number of locations only. At that moment, based on the aircraft data, Koinu might be relatively weak.

For the third flight, the flight level was lower and widespread hurricane force winds were recorded within the eyewall (Figure 2(c)). This is consistent with the weather radar observation

and satellite imagery estimation that Koinu was a severe typhoon. Unfortunately, data were only available at the western half of Koinu so that a full picture of the distribution of winds could not be obtained.

Dropsondes were released by the aircraft at a height of approximately 10 km to measure the vertical profiles of wind speed, wind direction, temperature, humidity, and pressure. The descriptions of the dropsondes are provided in Chan et al. (2018) and He et al. (2022). The ASPEN software was used to post-process the dropsonde data (Zhang et al., 2013). The available dropsonde data are analyzed in Figure 3 for radial wind speed, and Figure 4 for equivalent potential temperature. It could be seen from Figure 3 that the boundary layer of Koinu had good inflow, suggesting that Koinu might continue to intensify over the northeastern part of the South China Sea, as indicated by He et al. (2022). On the other hand, the equivalent potential temperature profiles did not show much instability in the atmospheric boundary layer, i.e. the equivalent potential temperatures were generally constant with height and sometimes even increasing with height. According to the results of He et al. (2022), this might suggest that the atmospheric instability was rather limited to favour further strengthening of Koinu at that moment. The filled contour plots of equivalent potential temperature with respect to pressure levels are presented in Figure 5. The warm core structure of the tropical cyclone similar to that shown in Emanuel (2018) is clearly depicted in the figure, which agrees with previous observations (He et al., 2022).

The vertical wind speed profiles from dropsondes on 6 October are shown in Figure 6. Similar to previous studies (e.g. He et al., 2022; He et al., 2023), Vickery model provides the best fit for the data points. The wind speed could be as high as around 33 m/s near the surface at a distance of about 24 km from the centre of Koinu.

The time series of the various meteorological parameters from the air data probe are shown in Figures 7 and 10 for the flight on the morning of 6 October, Figures 8 and 11 for the flight on the afternoon of 6 October, and Figures 9 and 12 for the flight on the morning of 7 October. The calculation of the turbulent kinetic energy (TKE) and eddy dissipation rate (EDR, ε) generally follow those in Zhang et al. (2011), Zhao et al. (2019), and He et al. (2023). Below are some observations in general: (a) in crossing/proximity of the eye of Koinu, the wind directions generally went through a circle and the wind speeds were rather low; (b) near the eye

of Koinu, the vertical velocity showed much fluctuations, and it could be both positive and negative, reaching around 5 m/s or more in magnitude; (c) the turbulence intensity parameters, namely, turbulent kinetic energy (TKE) and eddy dissipation rate (EDR), were generally the largest near the centre of Koinu; similar to previous study (He et al., 2023), TKE and EDR are highly correlated with each other. The slope is in the order of 1.6 and the y-intercept is around 4 to 6. Based on the limited number of samples collected so far with a restricted number of TCs, these parameters appear to be universal and applicable for the TCs under study.

4 Radar observations

The weather radars in Hong Kong well captured the structure of Koinu. From the 3-km height imagery, the eyewall of Koinu showed up very well within the radarscope (Figure 13(a) and Figure 14(a)). They serve as validation reference for testing of the capability of ocean radar in analysing the wind structure of Koinu. The ocean surface wind speed and direction patterns of Koinu corresponding to the time of weather radar imageries are shown in Figures 13(b) and 14(b). Although extracting ocean wave parameters from the second-order spectra of sea echoes from ocean radar measurements is very challenging to engineering applications (Barrick, 2008; Liu et al., 2007; Wu et al., 2003), recent advancements in the beam sampling method and retrieval algorithms improved the reliability of the derived wind and waves in TC situations (Li et al., 2012). By comparing ocean radar derived wind field with the weather radar pictures, it could be seen that the ocean radar wind data captured the locations of Koinu's eye very well. The difference in the eye fix was just about 10-20 km. The wind speeds derived from the ocean radar were also generally reasonable, though underestimated as compared with the actual observations.

On the morning of 7 October, maximum winds of around 20 m/s were found at a distance of about 24 km (Figure 13(b)) and 30 km from the centre (Figure 14(b)). Both hinted the radius of maximum wind of Koinu was of the order of 20-30 km. On the early morning of 8 October (Figure 14(b)), gale force winds generally prevailed over the measurement domain of the ocean radar. This wind pattern also appeared to be reasonable except that an annular ring of maximum wind speed near the centre of Koinu could not be depicted in the derived field. It is probably due

to the compact structure of Koinu and limitations in the scale resolved by the remote sensing technique and the retrieval algorithm.

Apart from the surface wind speed, ocean radar derived products also include significant wave height. On the morning of 7 October (Figure 15(a)), higher wave height of around 8 m was found to be associated with the strong south to southeasterly winds. Though actual observations are not available, such a pattern also appears to be reasonable. On the morning of 8 October (Figure 15(b)), the wave heights were generally about 6-8 m in the measurement domain. At both times, the wave heights were much lower (well below 2 m) near the centre of Koinu because of weaker winds. This is also reasonable.

As in the case of Saola (He et al., 2023), eddy dissipation rate (EDR) map could be obtained from the spectral width data of the weather radars. A sample EDR map is shown in Figure 16. Compared to Saola, this time the EDR is much lower, in the order of 0.3 to 0.35 at most. The turbulence was much lower on the eastern and southern parts of the rainband wrapping into the centre of Koinu.

5 Satellite observations

A SAR picture has been obtained when Koinu was located just to the south of Hong Kong. From Figure 17, it clearly showed that Koinu was a very compact storm. The SAR winds were directly obtained from the NOAA's STAR SOCD (Satellite Oceanography and Climatology Division) level-2 SAR data download site. The STAR SOCD TC products include the retrieved products from SAR images captured by different satellites, and the image shown in Figure 17 is the scene captured by the Canadian Space Agency's RCM3 (RADARSAT Constellation Mission). The RCM was launched on June 12, 2019, with the three identical satellites working in concert to achieve daily access to 90% of the world's surface. The comparison results could be found in Figure 17. It could be seen that the SAR winds and the buoy winds are well correlated, though the buoy winds are generally lower, because they are 10-minute mean winds whereas the SAR winds are instantaneous. The availability of SAR wind data greatly help the monitoring and provision of warning service for TCs.

6 Waterspout

Associated with the outer rainbands of Koinu, an intense radar echo with a maximum reflectivity over 53 dBZ developed near the Dangan islands (about 20 km south of Hong Kong) at about 08:25 UTC on 9 October 2023. It moved west steadily and displayed a comma shape at around 09:13 UTC based on 1.5° PPI scan of the Qiu Yu Tan Weather Radar (QYTWR) in Shenzhen (Figure 18(a)). Doppler wind field from QYTWR showed a velocity couplet of size less than 5 km (Figure 18(b)), suggesting the formation of a waterspout. The maximum reflectivity core was located at a height of around 2.5 km and the maximum radial velocity was above 20 m/s (Figure 18(c)). The vortex tube related to the waterspout reached a height of about 2 km. Tracing the radar echo with reflectivity greater than 53 dBz as a proxy of tracking the waterspout, it seemed to have a rather long lifespan of over 3 hours, and the echo finally weakened after around 11:00 UTC that evening. In Hong Kong, waterspout occurred mostly in the summer months from June to August mostly caused by convective weather. The waterspout brewed from the rainbands of Koinu in the month of October was a relatively rare event.

The waterspout associated with Koinu can be regarded as a TC spawned tornado. Carroll-Smith et al. (2023) and Edwards (2012) pointed out several factors favourable to the formation of TC tornadoes which were found applicable in this case. These included (i) the waterspout was formed over the northeastern quadrant relative to Koinu's centre due to climatologically enhanced instability and shear in that region, (ii) QYTWR's radar image (left panel of Figure 18(c)) suggested the presence of shallow-topped "miniature" supercell which was typically formed under high shear and helicity environment as well as concentration of buoyancy in the lowest few kilometres above ground, (iii) the presence of baroclinic boundaries (in this case the Dangan islands or broadly speaking the coastal areas of Guangdong) providing stronger horizontal temperature gradient and higher low-level shear for spawning tornado. Further, some of the precursor requirements for tornado touchdowns as mentioned in Schneider et al. (2007) were observed in this case including a hook shape signature in the radar reflectivity image (comma shape in Figure 18(a)) and the presence of a velocity enhancement signature (VES) of 30 kt (15.4 m/s) or greater in the height range of 2 to 4 km (right panel in Figure 18(c) with peak velocity greater than 20 m/s and height above 2 km) which was a stronger indicator of tornadogenesis. While TC-spawned tornado was seldomly observed near the south China coast, the meteorological factors contributing to the formation of waterspout related to Koinu were

found consistent with the results of past studies by Carroll-Smith et al. (2023), Schneider et al. (2007) and Edwards (2012).

7 Forecasting aspect

Koinu was very compact to be well resolved by the existing global numerical weather prediction models. Despite some early runs of the global models indicated that Koinu might cross the northern part of the South China Sea as a relatively strong TC, most global models subsequently changed their stories on a consensus that Koinu would rapidly weaken over the northeastern part of the South China Sea and quickly dissipate due to intrusion of drier and cooler air of the northeast monsoon. This might have misled operational forecasting and warning services that Koinu might not pose significant threat to the Pearl River Estuary, even as close as a few days before its closest approach. Nevertheless, the Pangu-Weather model persistently forecast that Koinu would continue to track west along the coastal areas of Guangdong and reach the Pearl River Estuary. As a result, they have much better performance in terms of track error, especially in the forecast period of 2 to 5 days, as shown in the time series plots of Figure 19.

In addition to Saola, this is the second time that AI-based models outperformed conventional models in forecasting the movement of a midget TC. The mesoscale model TRAM (Zhang et al., 2022) with a horizontal resolution of 9 km also performed much better than global models, in terms of both track forecast (Figure 19) and intensity forecast where multiple runs of TRAMS indicated an intense yet midget Koinu would manage to reach the Pearl River Estuary. This points to the need for improving the performance of global numerical weather prediction models in forecasting the intensity and movement of TCs.

8 Conclusions

Koinu was a difficult case for TC warning service due to its compact size and rather erratic movement over coastal waters of Guangdong. This paper documents the weather observations of Koinu from a number of platforms, including aircraft, radar and satellite. It is

hoped that the paper could stimulate further study of this case, particularly the possibility of forecasting the compact structure and erratic track of Koinu.

The dropsonde data indicated good inflow in the boundary layer, and the Vickery model provided the best fit for wind speed profiles. The warm core structure of the tropical cyclone was clearly depicted, while the equivalent potential temperature profiles showed limited atmospheric instability. The probe data revealed updraft and downdraft up to about 5 m/s, along with high turbulence near the storm center. A correlation between turbulent kinetic energy and eddy dissipation rate was observed. These findings contribute to our understanding of wind and turbulence structure of tropical cyclones.

The SAR picture obtained when Koinu was near Hong Kong revealed its compact nature. The SAR winds showed good correlation with buoy winds, albeit slightly lower due to different temporal scales. The weather radar observations suggest the occurrence of a waterspout in the vicinity of Koinu. Typical characteristics of a TC-spawned tornado were displayed, with factors such as enhanced instability and shear, presence of a shallow-topped supercell, and the influence of baroclinic boundaries. The observations align with previous studies on tornado formation in TCs.

Koinu's compact size posed challenges for global numerical weather prediction models, leading to inconsistencies in track forecasts. However, the Pangu-Weather model and the mesoscale TRAM model demonstrated better performance in forecasting Koinu's track and intensity. This highlights the importance of enhancing global models for accurate TC intensity and movement predictions.

Based on the results so far in the TC season of 2023, AI-based Pangu-Weather models were found to have outperformed the conventional models in forecasting the track and intensity of TCs. Rather urgent need would be required to improve such models in order to provide effective support to the provision of forecast and warning services of TCs in this part of the world.

Open Research

Availability Statement

The aircraft data used in the study are available at Zenodo via 10.5281/zenodo.10028903

Chan, P. W. (2023). Flight data for Severe Typhoon Koinu [Data set]. Zenodo. https://doi.org/10.5281/zenodo.10028903

References

Barrick, D. E. (2008). 30 Years of CMTC and CODAR. Proceedings of the IEEE/OES/CMTC Ninth Working Conference on Current Measurement Technology, 131-136.

Beswick, K. M., Gallagher, M. W., Webb, A. R., Norton, E. G., & Perry, F. (2008). Application of the Aventech AIMMS20AQ airborne probe for turbulence measurements during the Convective Storm Initiation Project. *Atmospheric Chemistry and Physics*, *8*, 5449-5463.

Bi, K., Xie, L., Zhang, H., Chen, X., Gu, X., & Tian, O. (2023). Accurate medium-range global weather forecasting with 3D neural networks. *Nature*, *619*, 533–538. https://doi.org/10.1038/s41586-023-06185-3

Carroll-Smith, D., Green, B. W., Edwards, R., Bai, L., Litta, A. J., Huang, X., Pattie, L., Overpeck, S., & McCaul Jr. E. W. (2023). Forecasting tropical cyclone tornadoes and impacts: Report from IWTC-X. *Tropical Cyclone Research Review*, *12*, 123-135. https://doi.org/10.1016/j.tcrr.2023.06.003

Chan, P. W. (2023). Flight data for Severe Typhoon Koinu [Data set]. Zenodo. https://doi.org/10.5281/zenodo.10028903

Chan, P. W., Choy, C. W., Chiu, Y. Y. (2023a). Observational study of Super Typhoon Saola in 2023 when it was close to Hong Kong. *Preprints*, 2023091688. https://doi.org/10.20944/preprints202309.1688.v1

Chan, P. W., He, Y. H., Lui, Y. S. (2023b). Super Typhoon Saola (2309) affecting Hong Kong in September 2023–Forecasting Aspect. *Preprints*, 2023091634. https://doi.org/10.20944/preprints202309.1634.v1

Chan, P. W., Hon, K. K., & Foster, S. (2011). Wind data collected by a fixed-wing aircraft in the vicinity of a tropical cyclone over the south China coastal waters. *Meteorologische Zeitschrift*, *20*, 313-321.

Chan, P. W., Wu, N. G., Zhang, C. Z., Deng, W. J., & Hon, K. K. (2018). The first complete dropsonde observation of a tropical cyclone over the South China Sea by the Hong Kong Observatory. *Weather*, *73*, 227-234.

Deaves, D. M., & Harris, R. I. (1978). A Mathematical Model of the Structure of Strong Winds, CIRIA Report 76. London, the United Kingdom.

Edwards, R. (2012). Tropical Cyclone Tornadoes: A review of knowledge in research and prediction. *Electronic Journal of Severe Storms Meteorology*, *7*, 1-61. https://doi.org/10.55599/ejssm.v7i6.42

Emanuel, K. (2018). 100 years of progress in tropical cyclone research. *Meteorological Monographs*, *59*, 15.1-15.68. https://doi.org/10.1175/AMSMONOGRAPHS-D-18-0016.1

Gryning, S. E., Batchvarova, E., Brümmer, B., Jørgensen, H., & Larsen, S. (2007). On the extension of the wind profile over homogeneous terrain beyond the surface boundary layer. *Boundary-Layer Meteorology*, *124*, 251-268. https://doi.org/10.1007/s10546-007-9166-9

He, J. Y.; Chan, P.W.; Chan, Y. W.; & Cheung, P. (2023). Super Typhoon Saola (2023) over the northern part of the South China Sea – aircraft data analysis. *Preprints*, 2023091683. https://doi.org/10.20944/preprints202309.1683.v1

He, J. Y., Hon, K. K., Chan, P. W., & Li, Q. S. (2022). Dropsonde observations and numerical simulations for intensifying and weakening tropical cyclones over the northern part of the South China Sea. *Weather*, *77*, 332-338. https://doi.org/10.1002/wea.4123

Li, L., Wu, X., Li, Y., Long L., Liu, B., Xu, X., Chen, M., & Xue, C. (2012). Ocean surface wind and wave monitoring at Typhoon Fung-Wong by HFSWR OSMAR071, *Journal of Remote Sensing*, *16*, 154-159.

Liu, L., Wu, X. B., Chen, F., Yang, S.L., & Ke, H. Y. (2007). Algorithm for HF radar vector current measurements. *Journal of Oceanography*, *63*, 47-66. https://doi.org/10.1007/s10872-007-0005-x

Schneider, D., & Sharp, S. (2007). Radar signatures of tropical cyclone tornadoes in central north Carolina. *Weather and Forecasting*, *22*, 278-286. https://doi.org/10.1175/WAF992.1

Vickery, P. J., Wadhera, D., Powell, M. D., & Chen, Y. (2009). A hurricane boundary layer and wind field model for use in engineering applications. *Journal of Applied Meteorology and Climatology*, *48*, 381-405. https://doi.org/10.1175/2008JAMC1841.1

Wu, X. B., Yang, Z. L., Cheng, F., Wu, Z. C., Yang, Z. J., Wen, B. Y., Shi, Z. F., Tian, J. S., Hou, J. C., Ke, H. Y., & Gao, H.T. (2003). Ocean surface currents detection at the eastern China sea by HF surface wave radar. *Chinese Journal of Geophysics*, *46*, 340-346.

Zhang, J. A., Marks, F. D., Montgomery, M. T., & Lorsolo, S. (2011). An estimation of turbulent characteristics in the low-level region of intense hurricanes Allen (1980) and Hugo (1989). *Monthly Weather Review*, *139*, 1447-1462.

Zhang, J. A., Rogers, R. F., Reasor, P. D., Uhlhorn, E. W., & Marks, F. D. (2013). Asymmetric hurricane boundary layer structure from dropsonde composites in relation to the environmental vertical wind shear. *Monthly Weather Review*, *141*, 3968-3984.

Zhang, Y., Xu, D., Chen, Z., Meng, W. (2022). Offline diagnostics of skin sea surface temperature from a prognostic scheme and its application in typhoon forecasting using the CMA-TRAMS Model over south China. *Atmosphere*, *13*, 1324. https://doi.org/10.3390/atmos13081324

Zhao, Z., Chan, P. W., Wu, N., Zhang, J. A., & Hon, K. K. (2019). Aircraft observations of turbulence characteristics in the tropical cyclone boundary layer. *Boundary-Layer Meteorology*, *174*, 493-511.

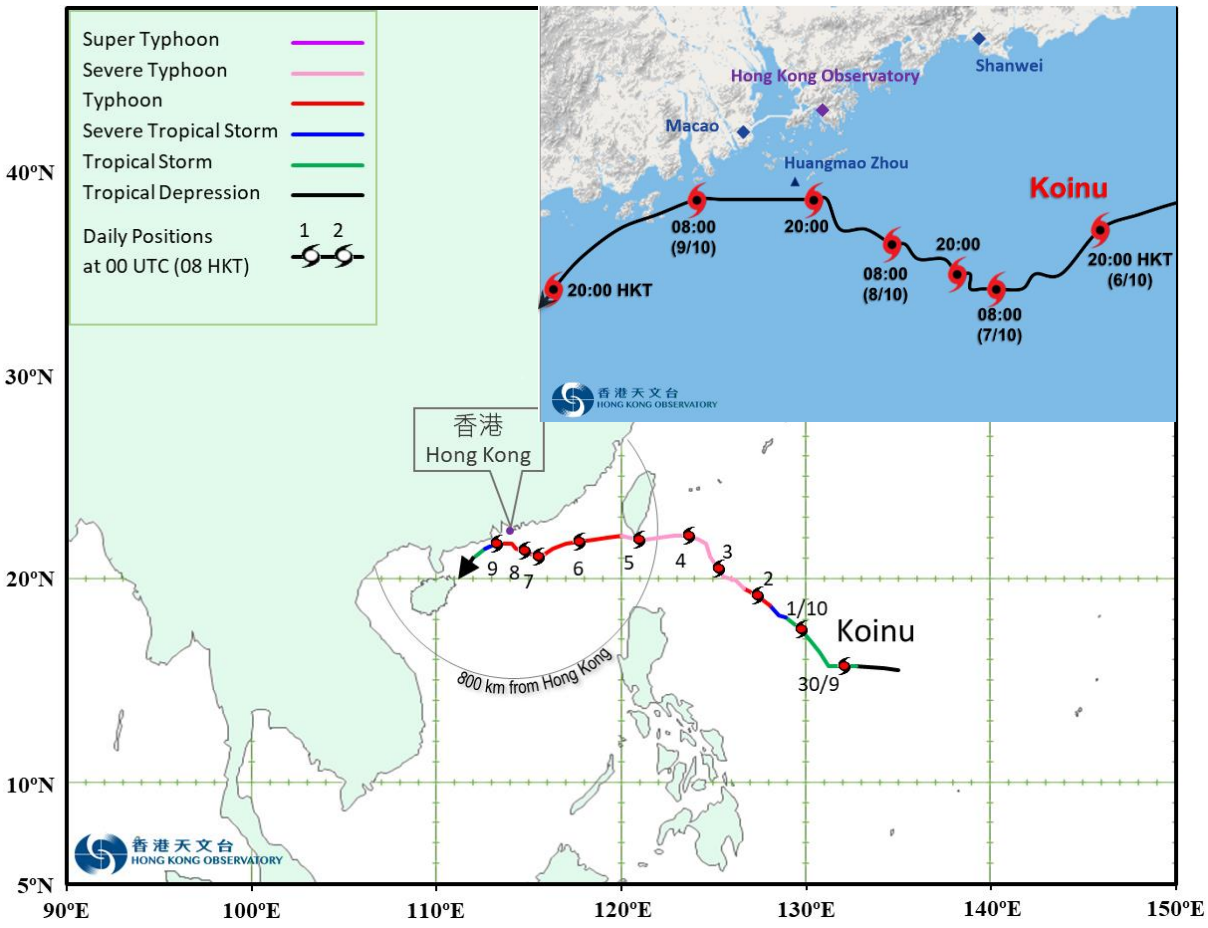

Figure 1. Provisional best track of Koinu and its track near Hong Kong (in Hong Kong Time (HKT) = UTC + 8 hours). The track of Koinu was slow and erratic during 6 – 8 October 2023. The centre of Koinu passed very close to Huangmao Zhou on the night of 8 October 2023.

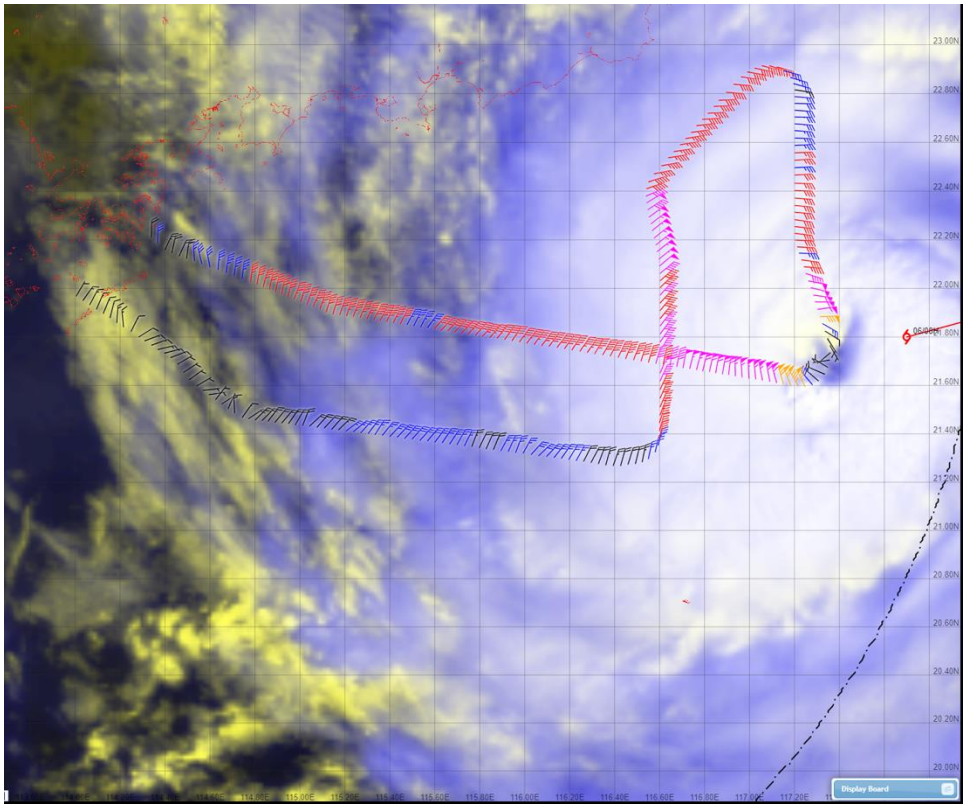

(a)

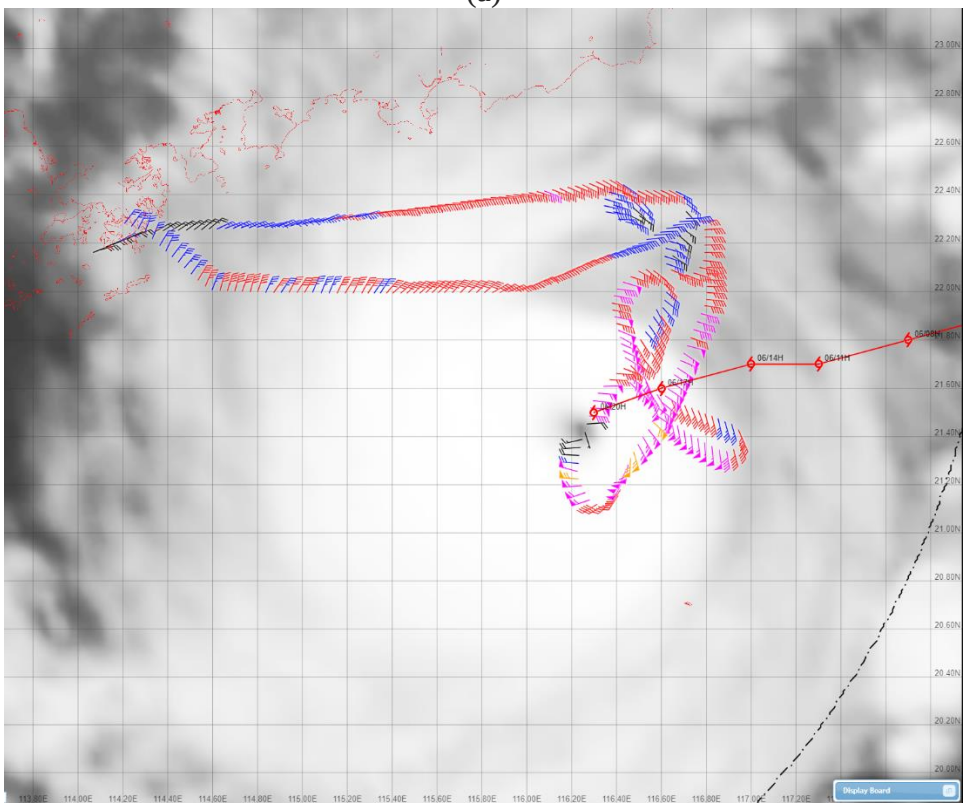

(b)

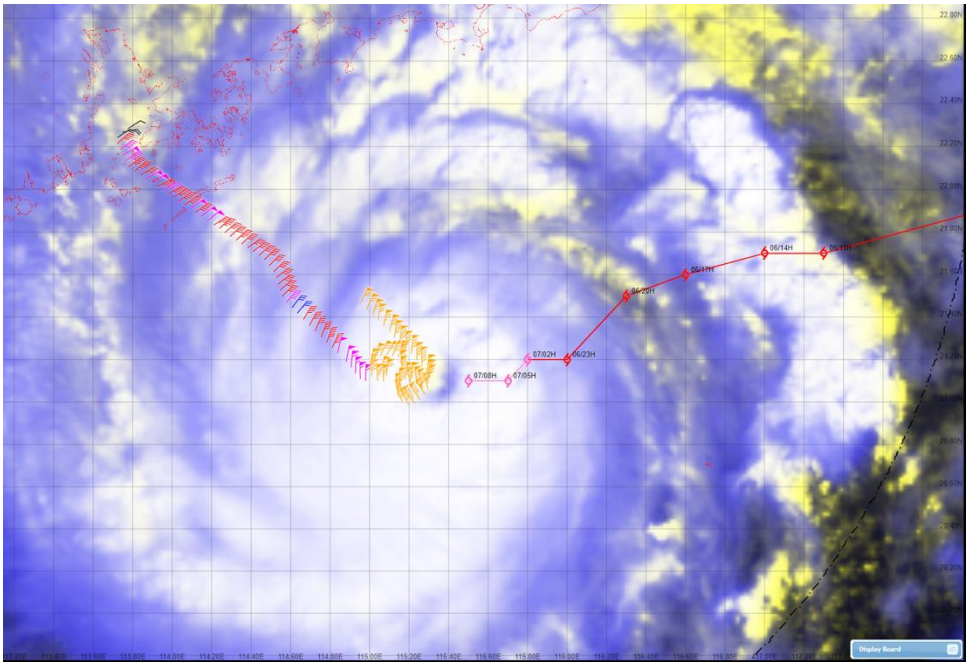

(c)

Figure 2. Flight routes and selected horizontal wind data along the flights overlaid on images generated from Himawari-9 geostationary satellite of Japan Meteorological Agency. (a) Flight between around 02:00 and 03:30 UTC, 6 October 2023 on top of false colour satellite image of 02 UTC; (b) flight between around 11:20 and 13:40 UTC, 6 October 2023 on top of infra-red satellite image of 12 UTC; and (c) flight between around 01:40 and 02:35 UTC, 7 October 2023, on top of false colour satellite image of 02 UTC.

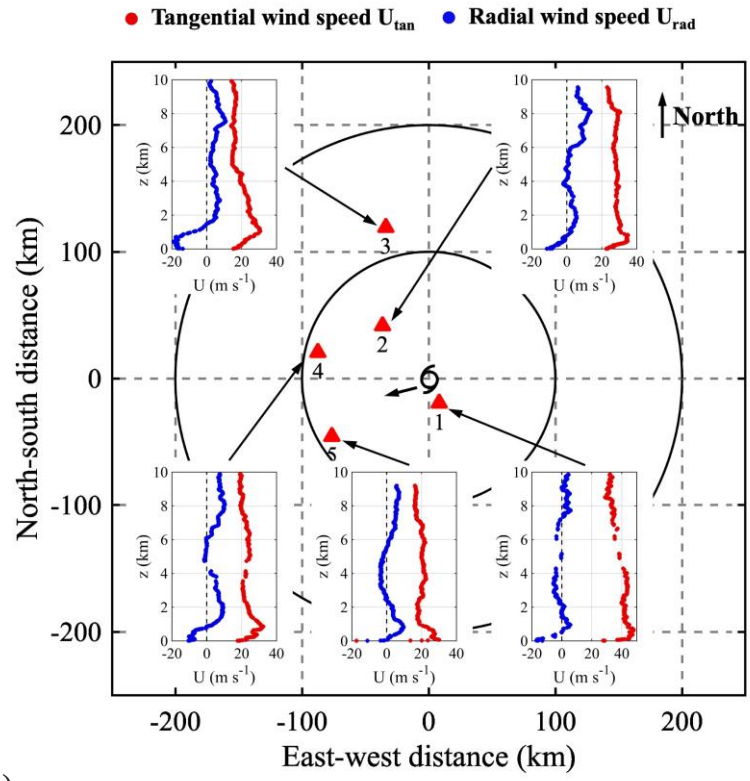
Tangential wind speed U_{tan}
Radial wind speed U_{rad}
North
North-south distance (km)
East-west distance (km)
z (km)
U (m s^{-1})
1
2
3
4
5
6

(a)

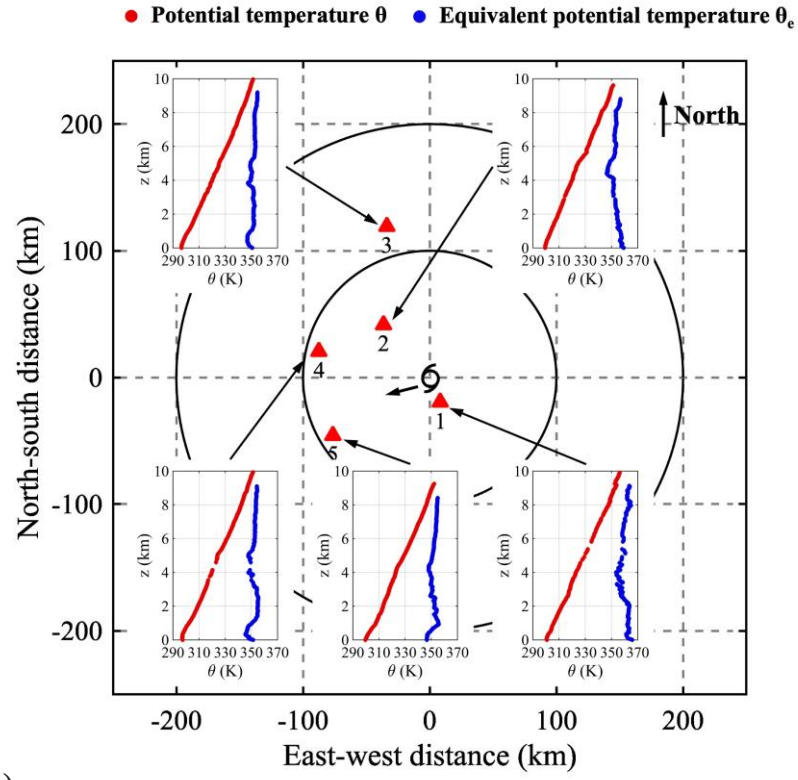
Potential temperature θ
Equivalent potential temperature $θ_e$
North
North-south distance (km)
East-west distance (km)
z (km)
θ (K)
1
2
3
4
5
6

(b)

386 **Figure 3**. (a) Vertical profiles of tangential (red) and radial (blue) wind speeds in Typhoon
387 Koinu at 0300UTC 6 October 2023. Tangential wind speed: anti-clockwise positive; radial wind
388 speed: outflow positive. Red triangles represent dropsonde locations relative to the storm center.
389 (b) Same as (a) but for potential temperature (red) and equivalent potential temperature (blue).
390

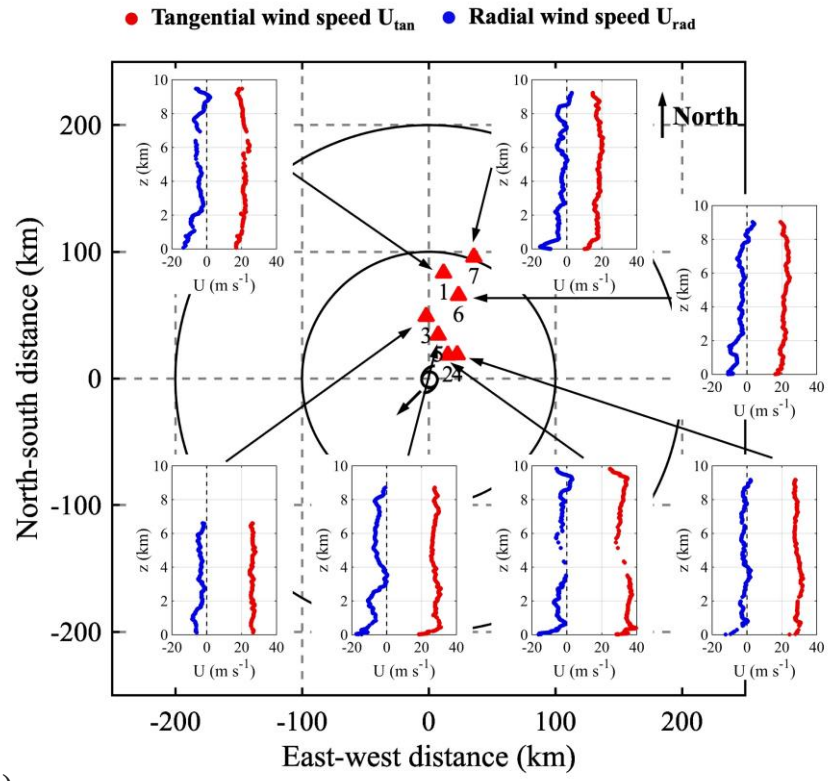
Tangential wind speed U_{tan}
Radial wind speed U_{rad}
North
North-south distance (km)
East-west distance (km)
z (km)
U (m s^{-1})
1
2
3
4
5
6
7

391 (a)

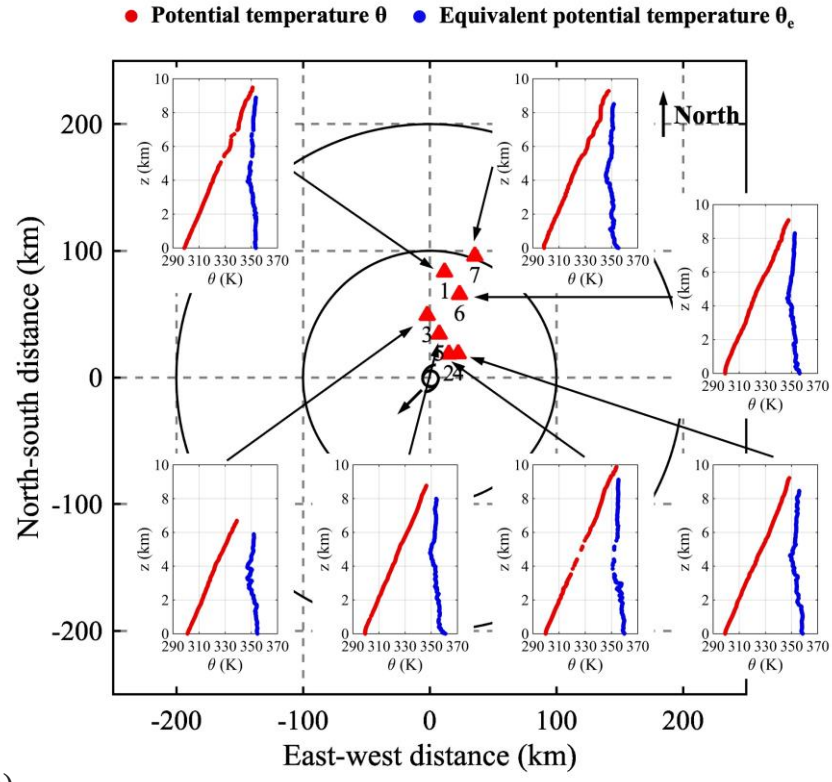
Potential temperature θ
Equivalent potential temperature $θ_e$
North
North-south distance (km)
East-west distance (km)
z (km)
θ (K)
1
2
3
4
5
6
7

392 (b)

393 **Figure 4**. Same as Figure 3 but for observations at 1200UTC 6 October 2023.
394

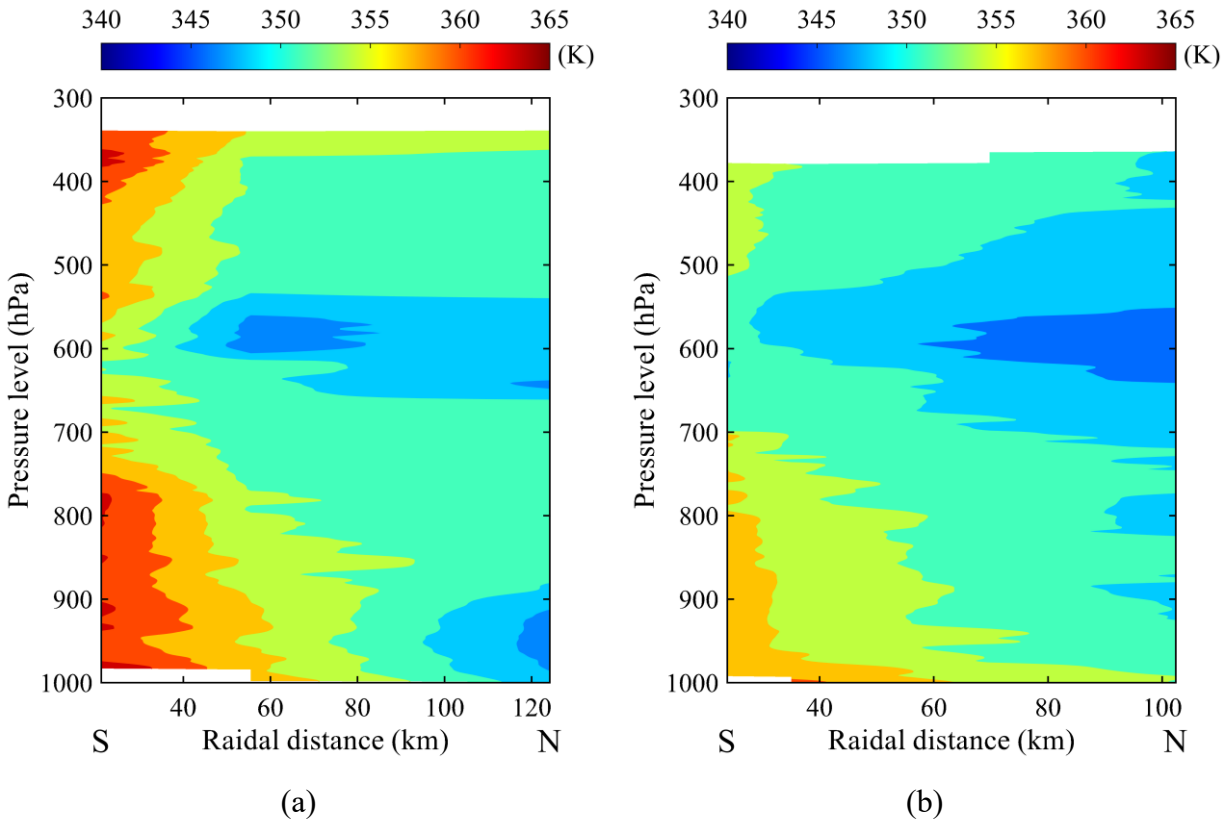

395 **Figure 5**. Contour plot of equivalent potential temperature θ_e (in K) in Typhoon Koinu, (a)
396 section observed by dropsondes "1-2-3" at 0300UTC 6 October 2023, and (b) section observed
397 by dropsondes "2-5-6-7" at 1200UTC 6 October 2023.
398

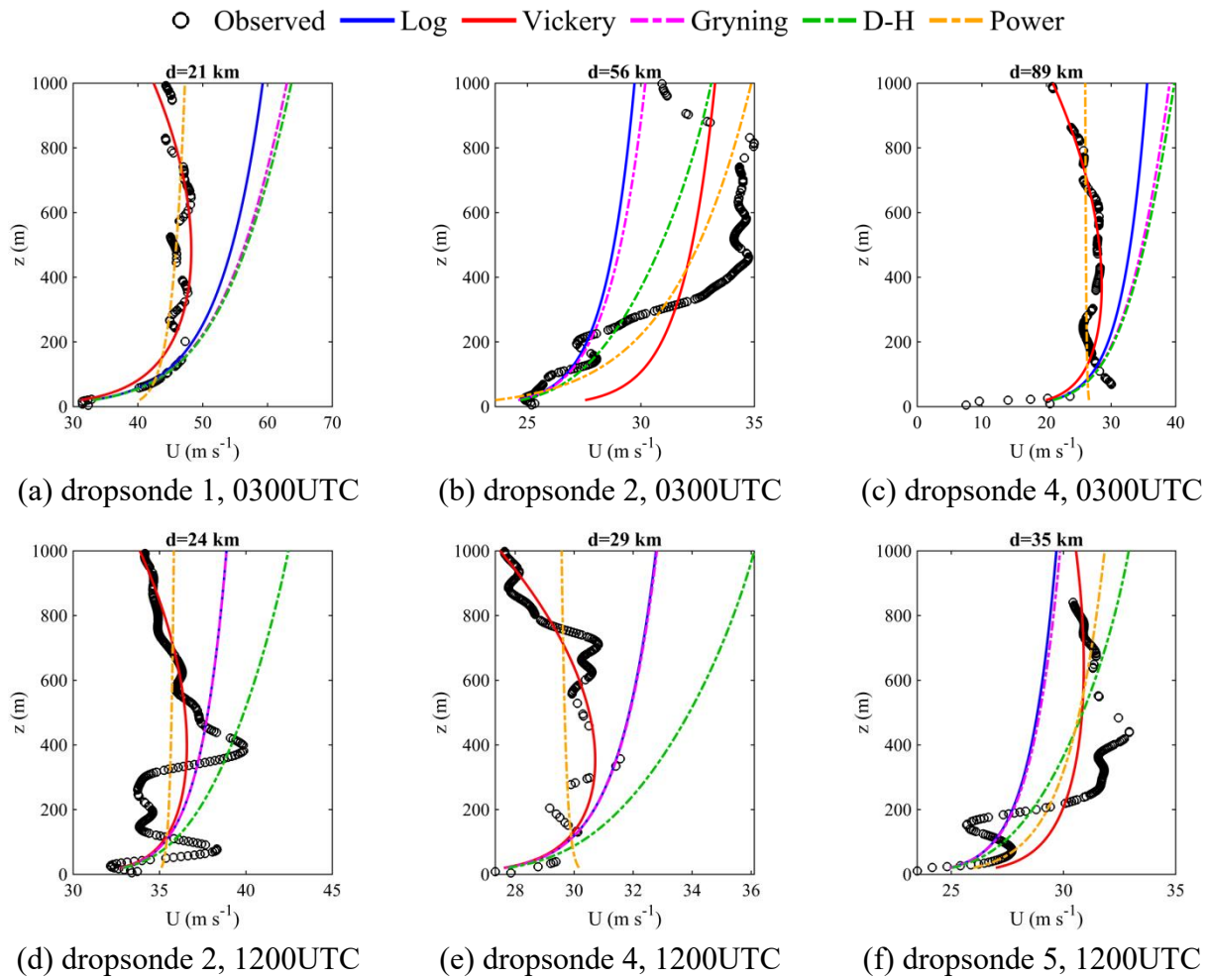

(a) dropsonde 1, 0300UTC (b) dropsonde 2, 0300UTC (c) dropsonde 4, 0300UTC

(d) dropsonde 2, 1200UTC (e) dropsonde 4, 1200UTC (f) dropsonde 5, 1200UTC

Figure 6. Fitting of vertical profiles of wind speeds in the lowest 1000 m in Typhoon Koinu to the wind profile models, including the logarithmic law, Vickery et al. (2009) model, Gryning et al. (2007) model, Deaves & Harris (1978) model, and power law, (a-c) at 0300UTC 6 October 2023 and (d-f) at 1200UTC 6 October 2023. d represents the distance to the storm center..

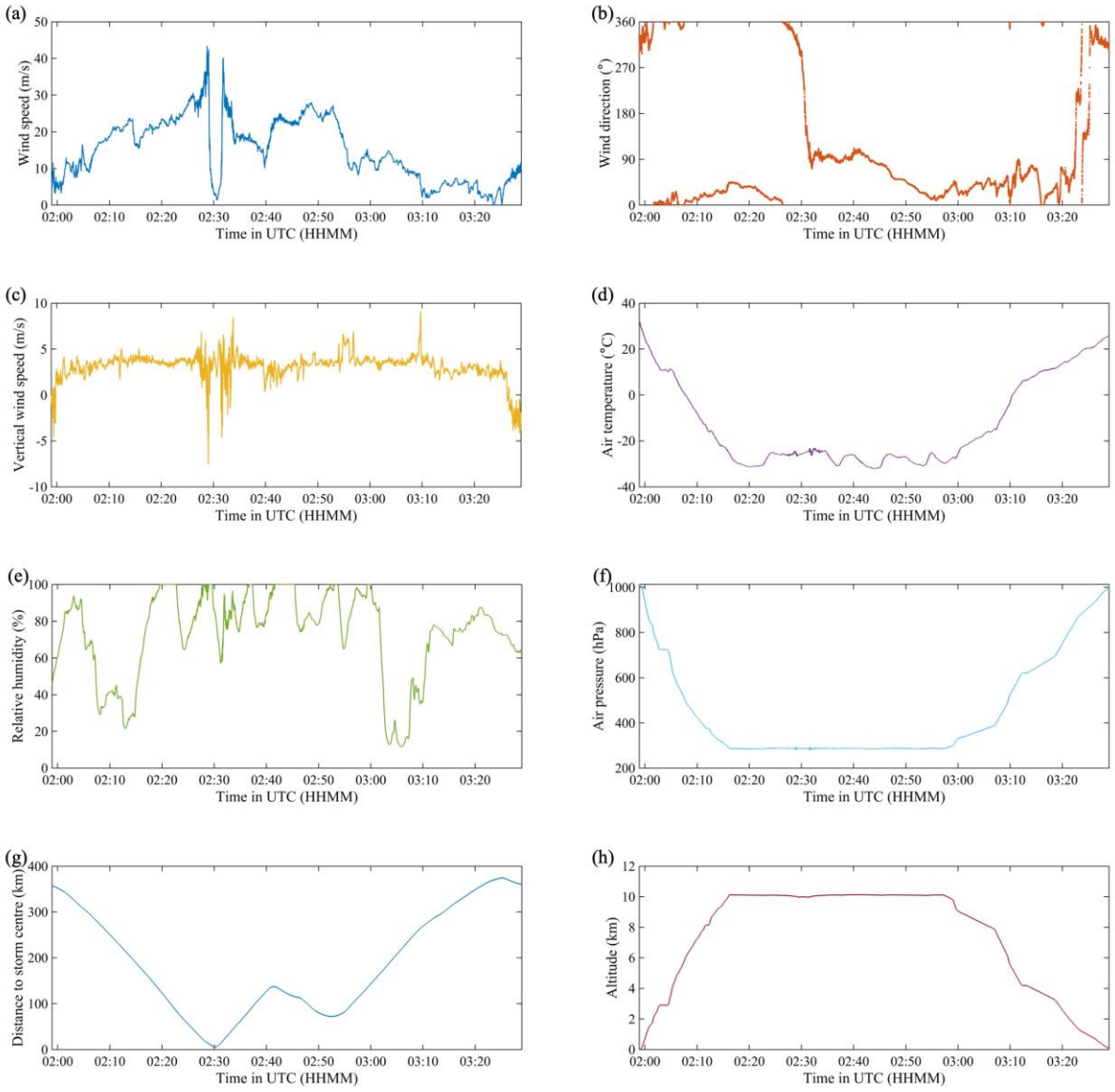

Figure 7. Time series of the (a) wind speed, (b) wind direction, (c) vertical wind speed, (d) air temperature, (e) relative humidity, (f) air pressure, (g) flight altitude, and (h) distance to storm centre based on the aircraft data in Typhoon Koinu between 0200 and 0330UTC 6 October 2023.

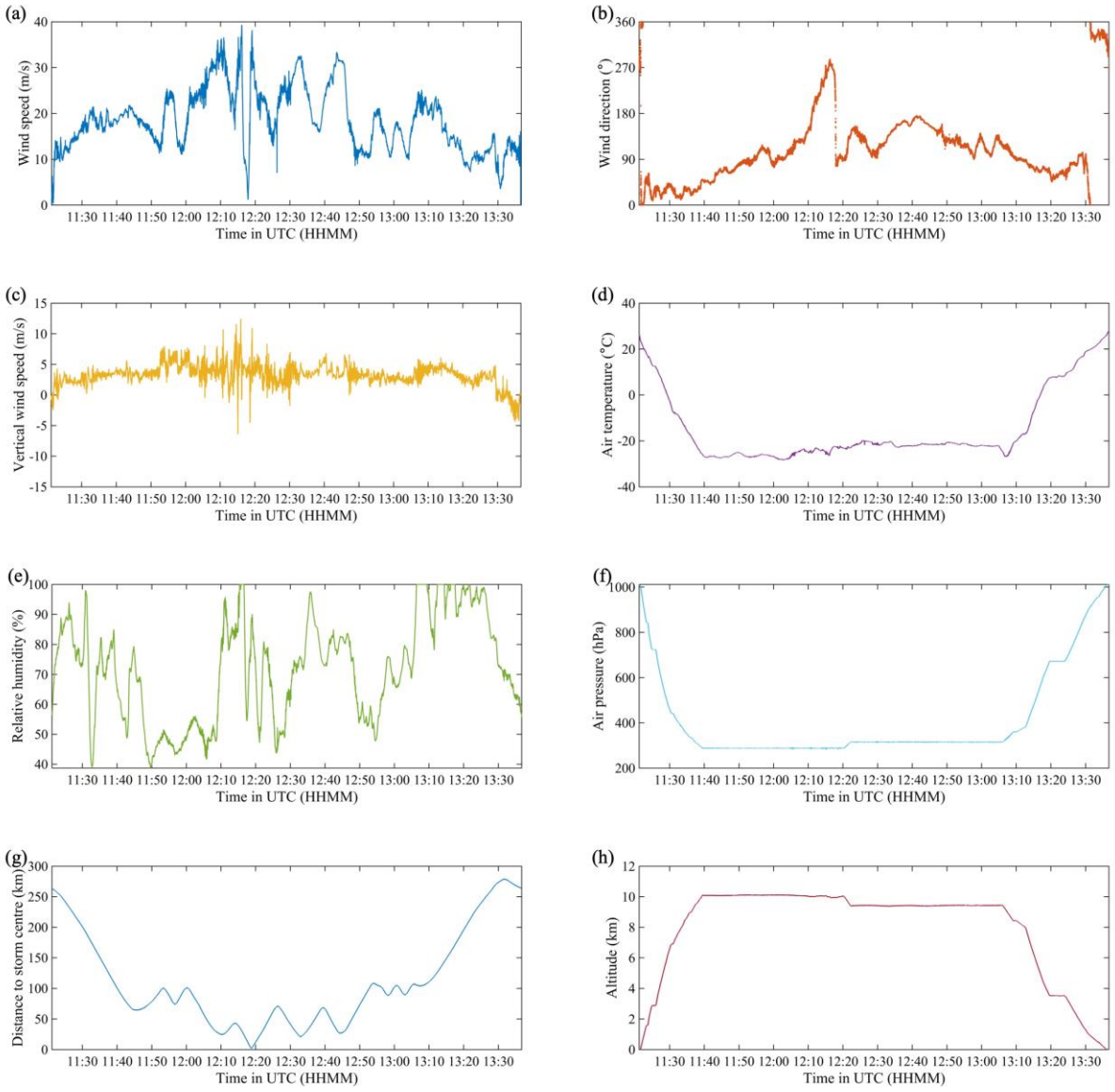

Figure 8. Same as Figure 7 but for observations between 1130 and 1330UTC 6 October 2023.

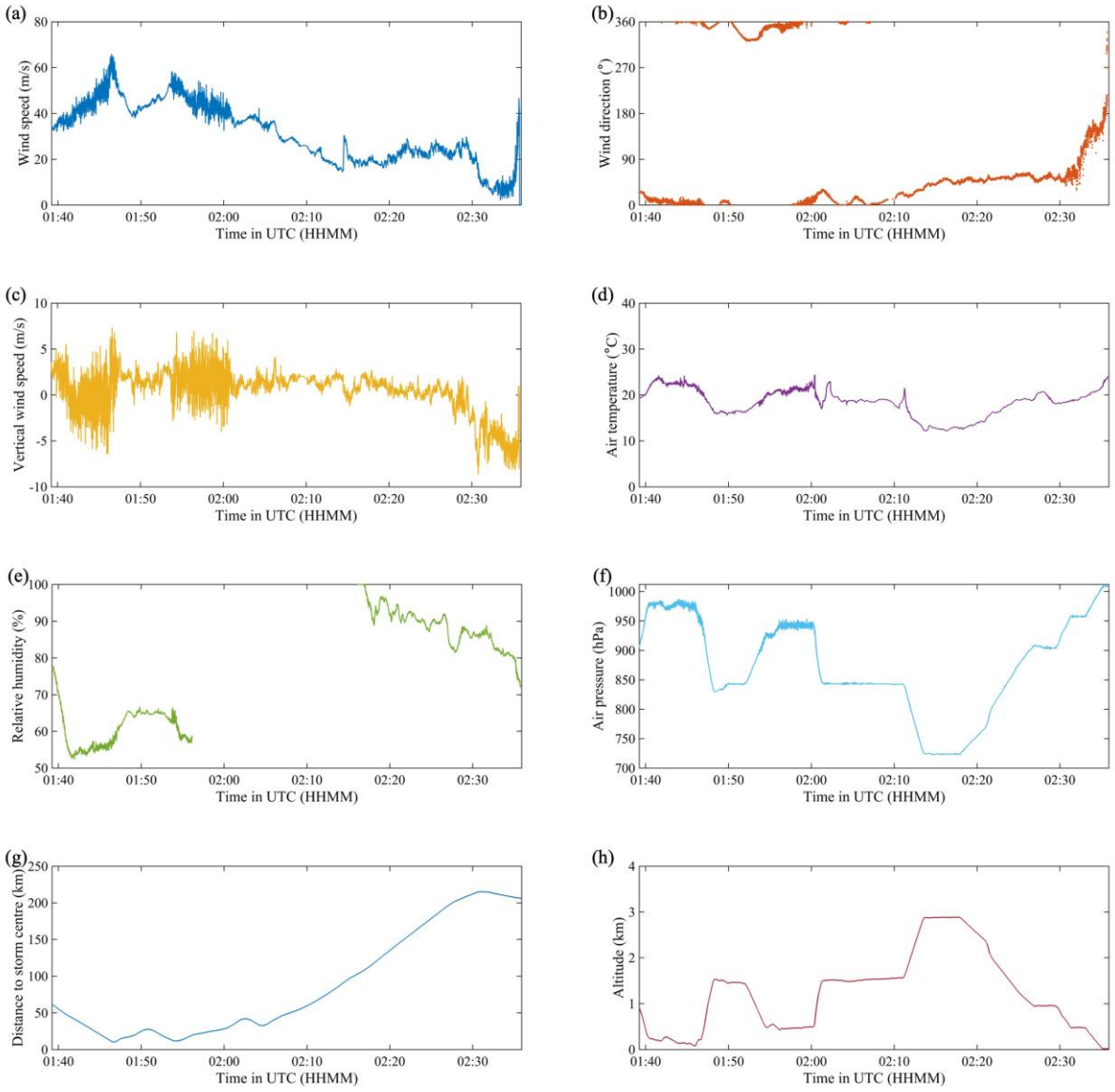

Figure 9. Same as Figure 7 but for observations between 0140 and 0240UTC 7 October 2023. The relative humidity data was missing between 0156 and 0215 due to device malfunction.

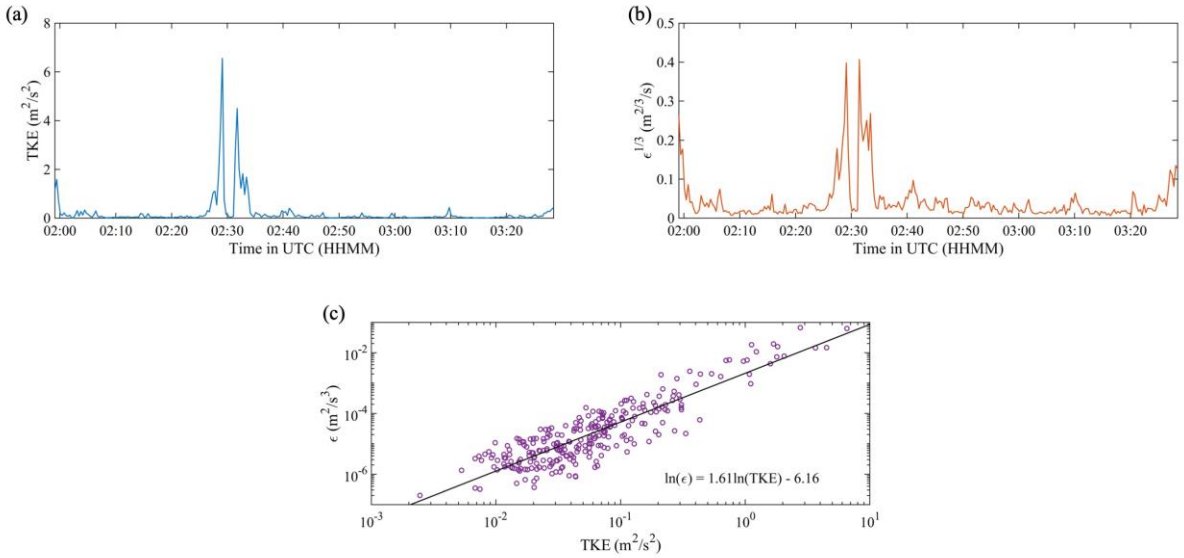

Figure 10. (a) Time series of the turbulent kinetic energy (TKE), (b) time series of the cube root of the eddy dissipation rate ($\varepsilon^{1/3}$), and (c) variation of ε with TKE, based on the aircraft data in Typhoon Koinu between 0200 and 0330UTC 6 October 2023. The black line in (c) represents the linear fit between ln(ε) and ln(TKE).

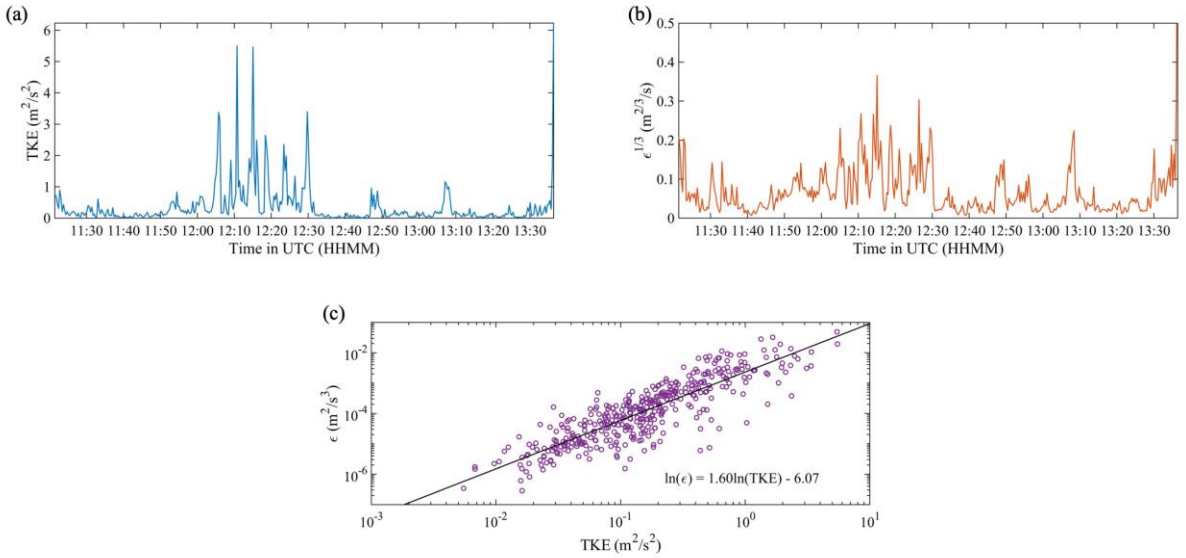

422

423 **Figure 11**. Same as Figure 10 but for observations between 1130 and 1330UTC 6 October 2023.
424

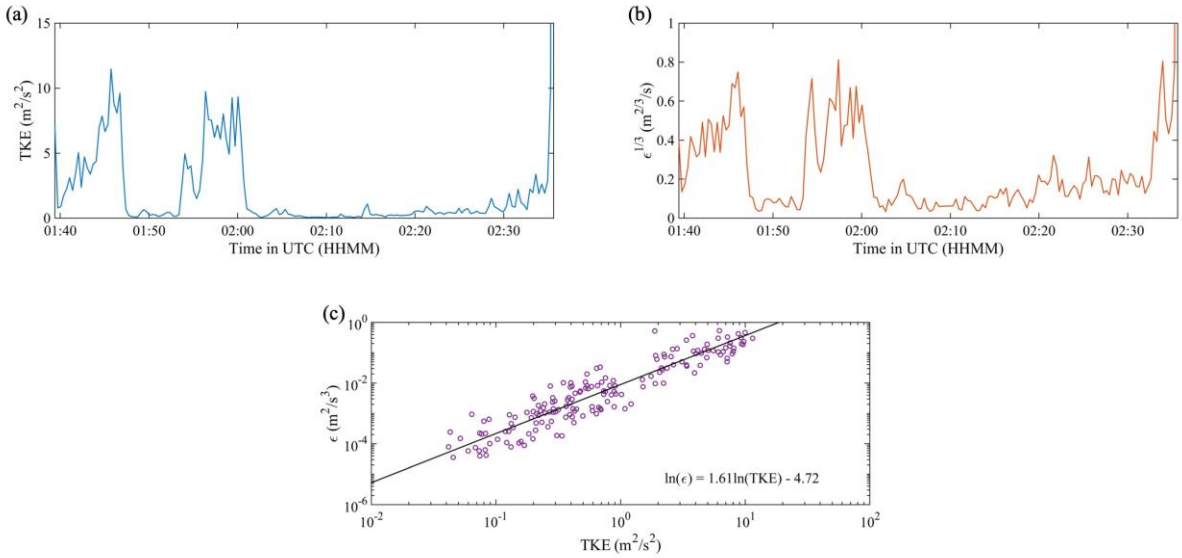

425

426 **Figure 12**. Same as Figure 10 but for observations between 0140 and 0240UTC 7 October 2023.
427

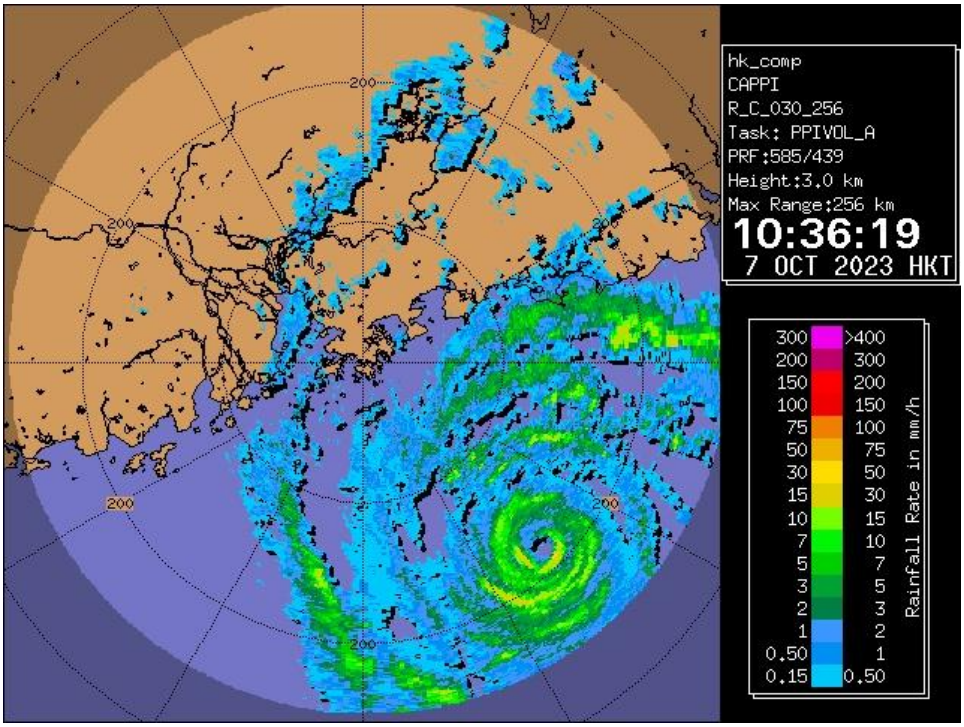

(a)

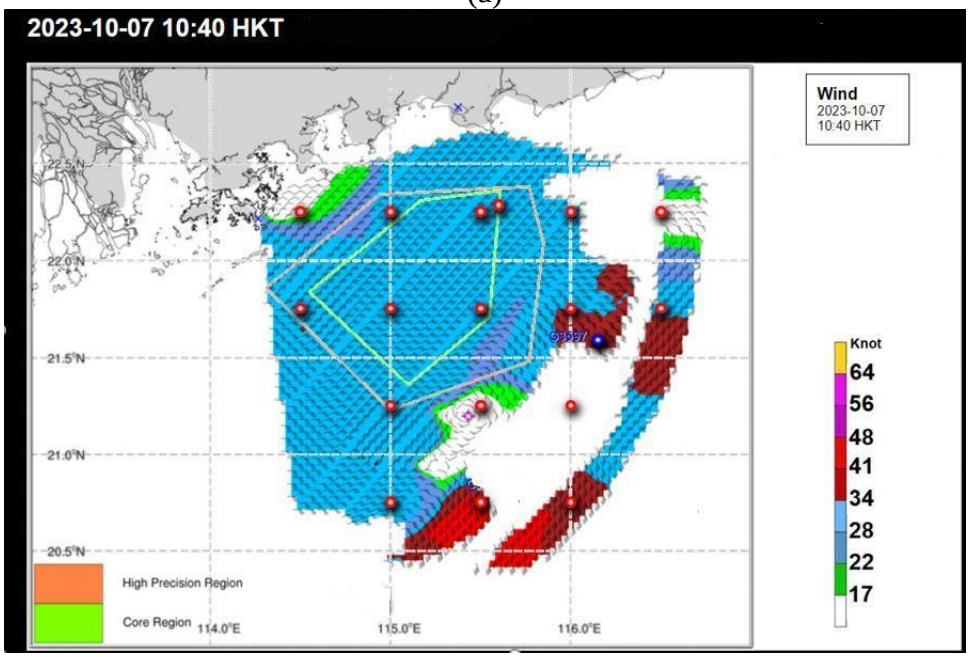

(b)

Figure 13. (a) Weather radar imagery at 3-km CAPPI showing Koinu's eye near 21.1N, 115.4E at around 02:36 UTC on 7 October 2023 ; (b) wind field derived from ocean radar around the same time also indicating an eye (purple star) at around 21.2N, 115.4E.

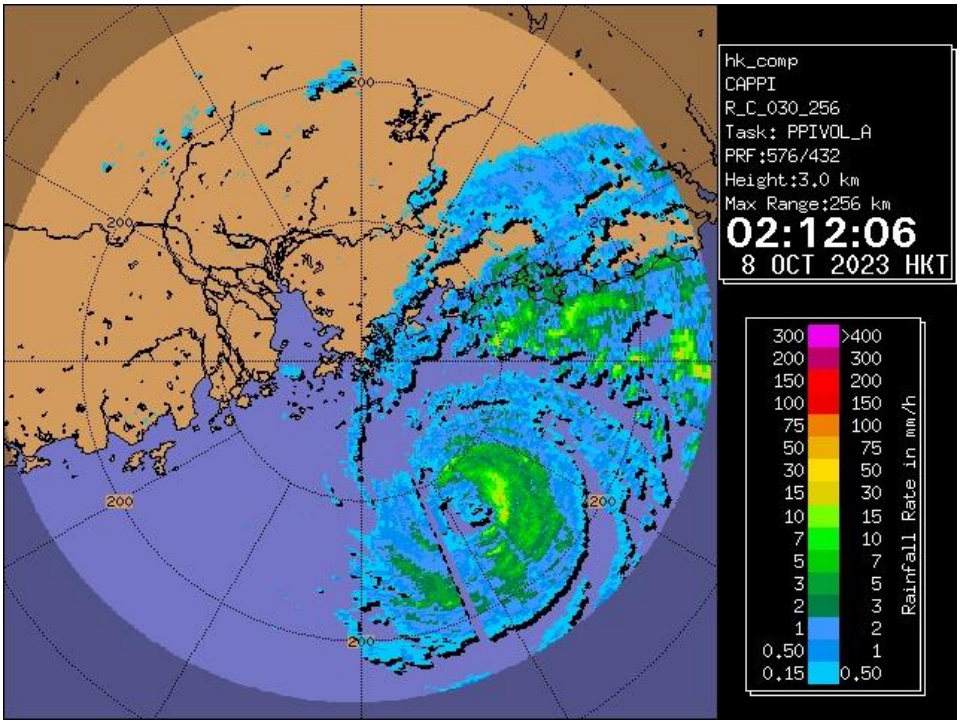

(a)

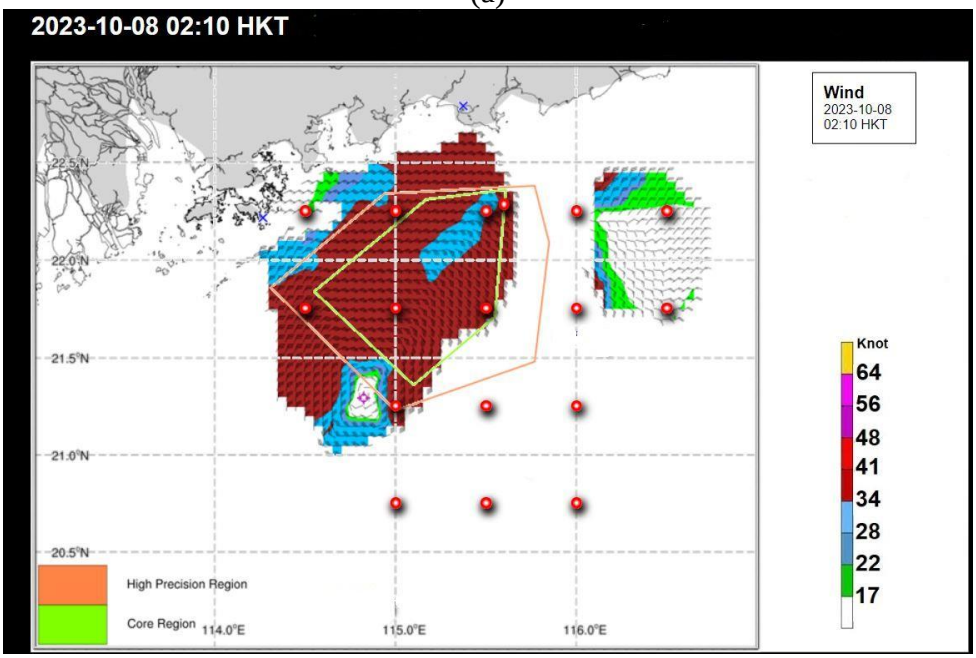

(b)

Figure 14. (a) Weather radar imagery at 3-km CAPPI showing Koinu's eye near 21.4N, 115.0E at around 18:12 UTC on 7 October 2023; and (b) wind field derived from ocean radar around the same time also indicating an eye (purple star) at around 21.3N, 114.8E.

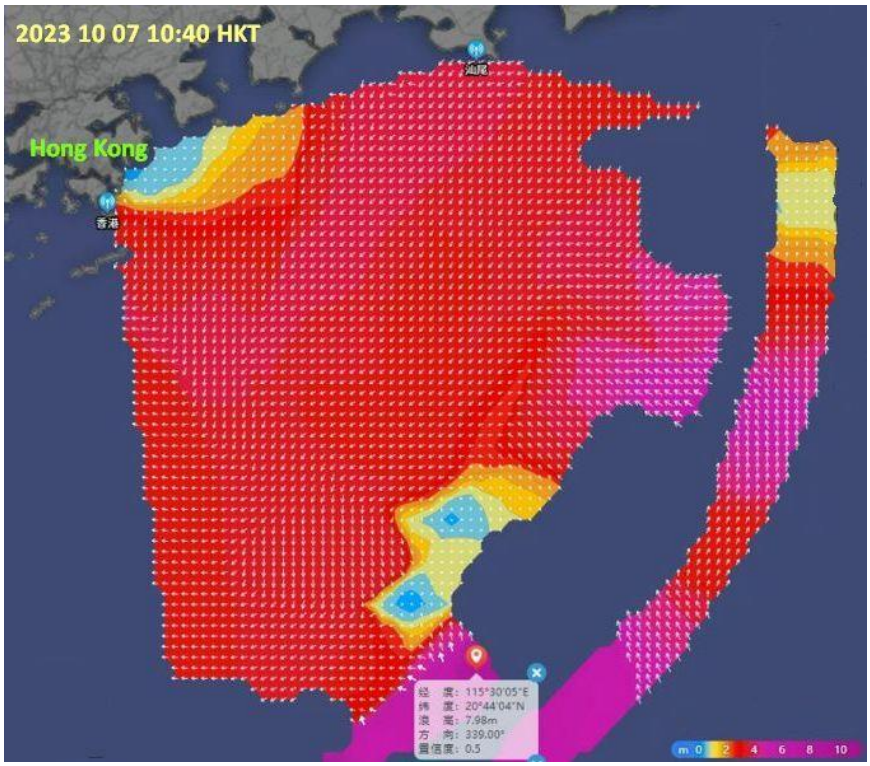

(a)

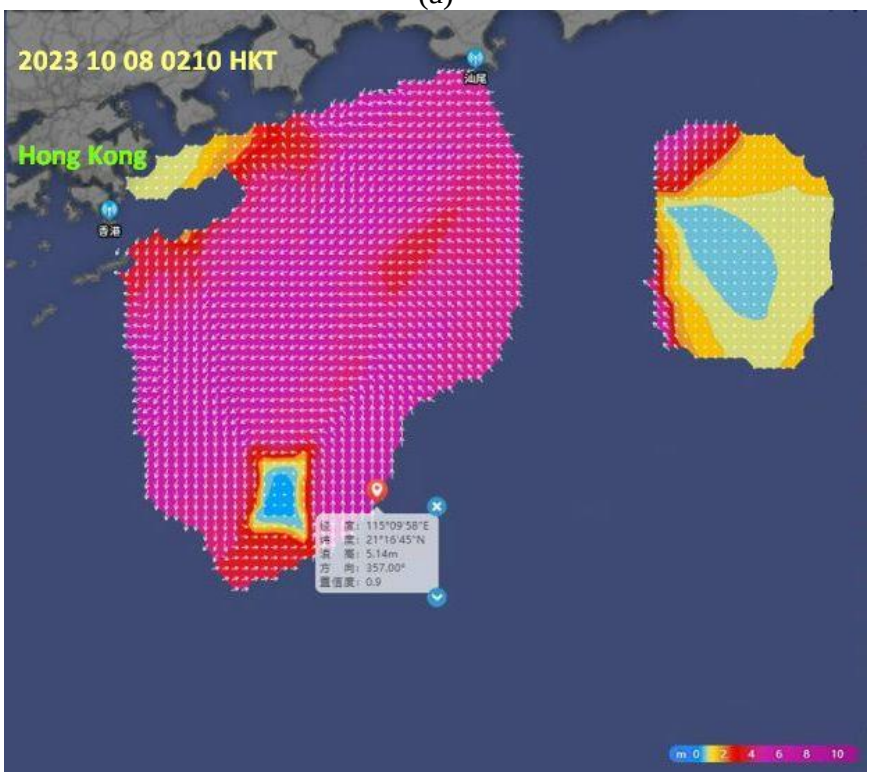

(b)

Figure 15. Significant wave height derived from ocean radar at (a) 02:40 UTC; and (b) 18:10 UTC on 7 October 2023.

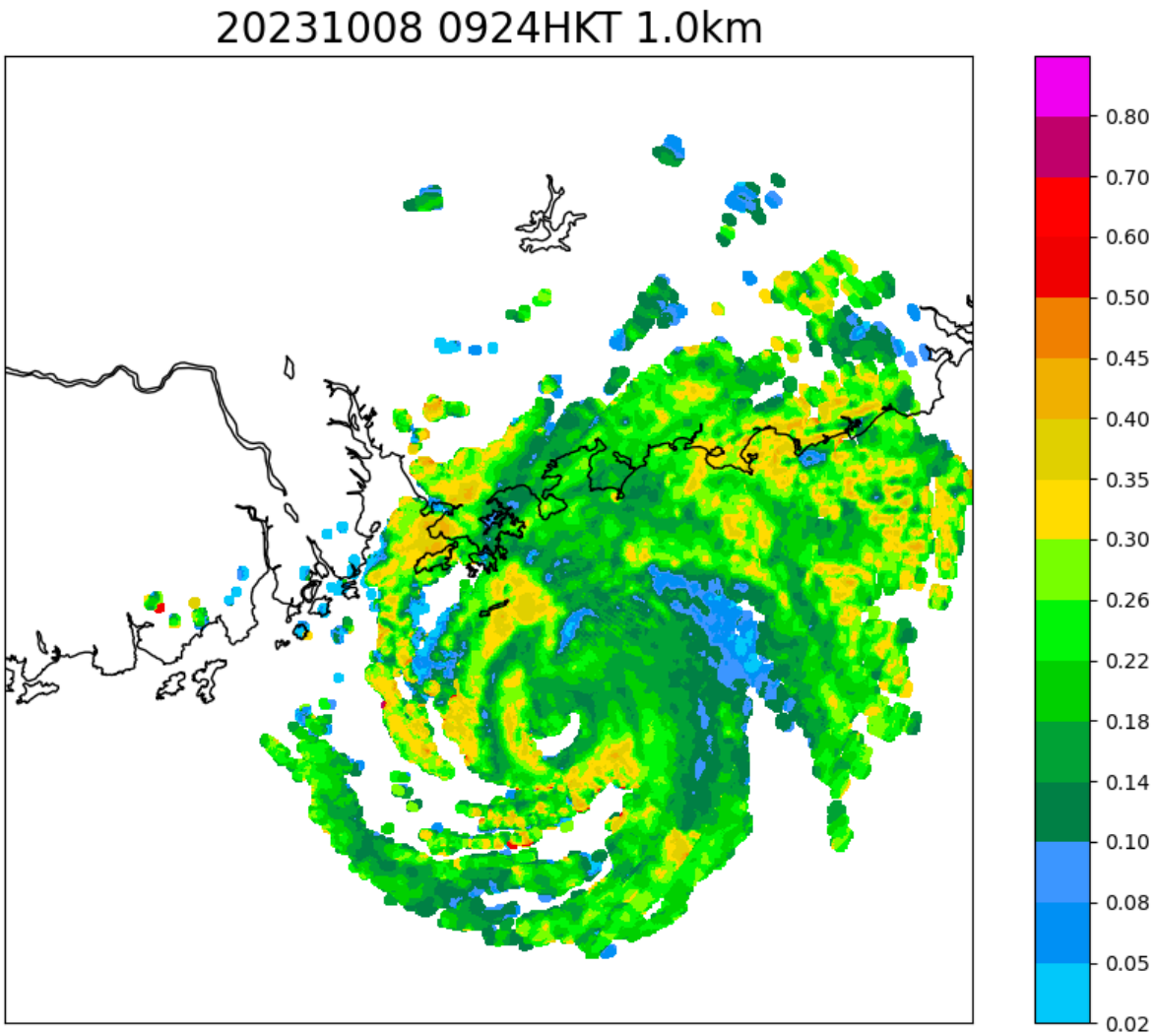

Figure 16. EDR (m^2/s^3) map of Koinu at 01:24 UTC 8 October 2023.

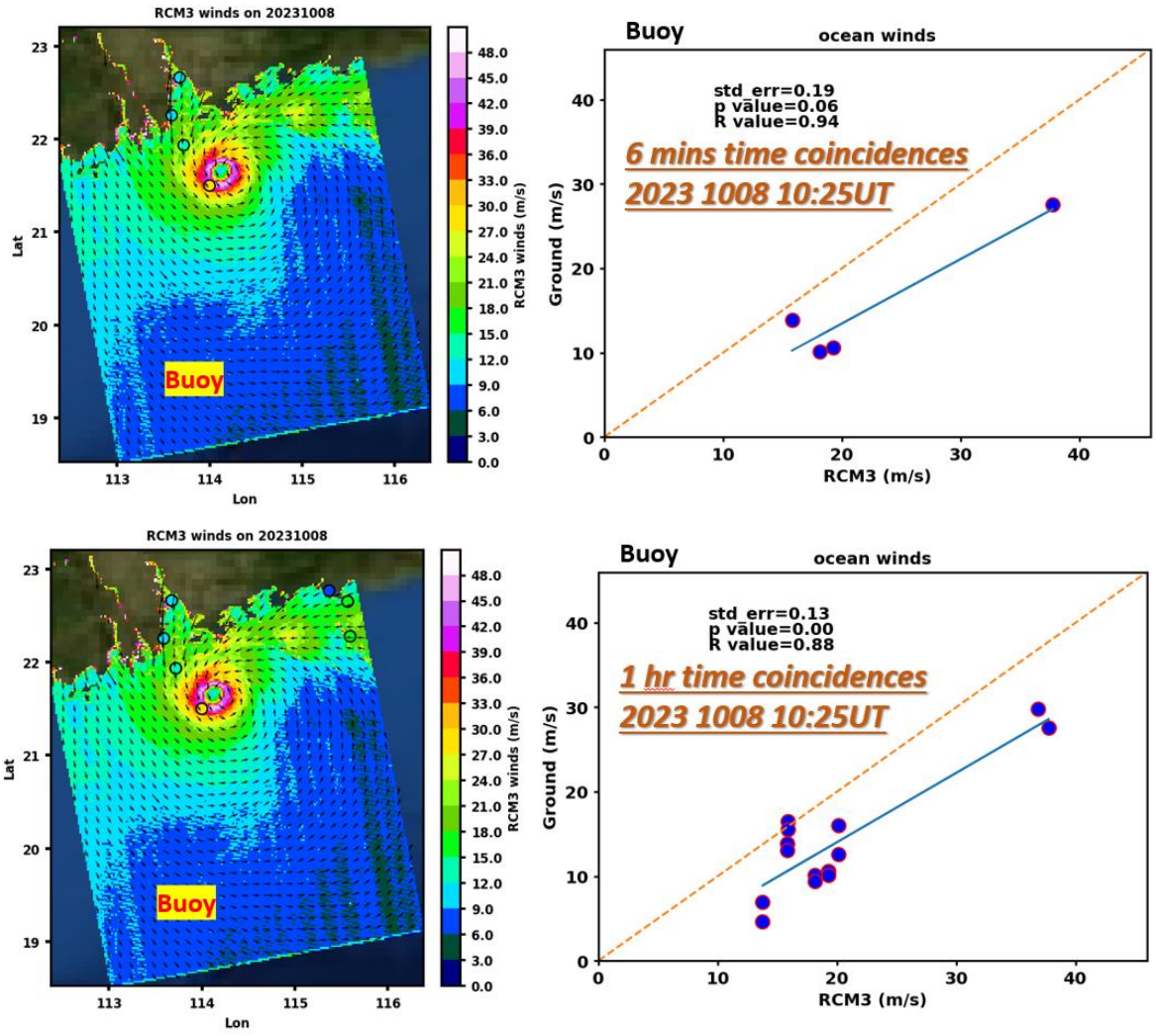

Figure 17. SAR winds captured by Canadian Space Agency's RADARSAT Constellation Mission (RCM3) on 8 October 2023 (left). Comparison of ocean winds between RCM3 winds and buoy observations (right).

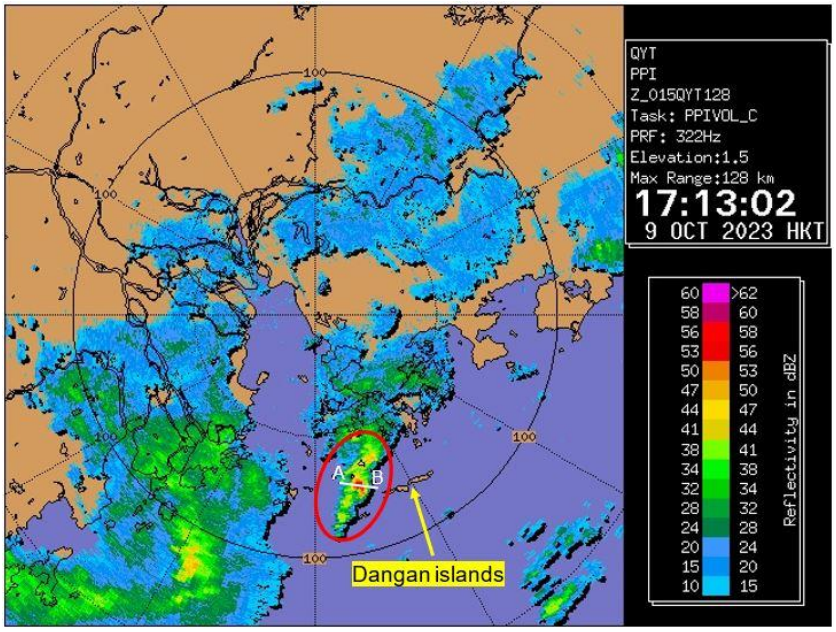
QYT
PPI
Z_015QYT128
Task: PPIVOL_C
PRF: 322Hz
Elevation:1.5
Max Range:128 km
17:13:02
9 OCT 2023 HKT
Reflectivity in dBZ
A
B
Dangan islands

(a)

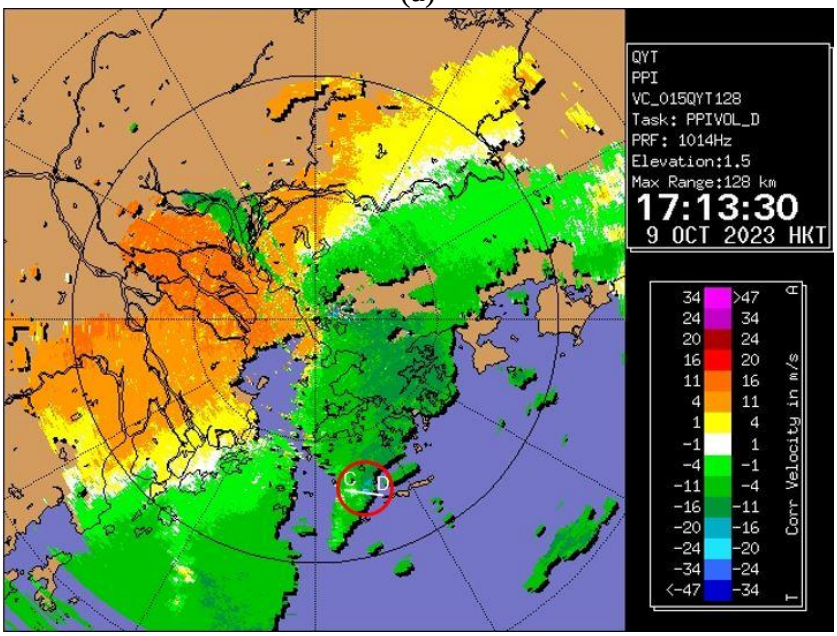
QYT
PPI
VC_015QYT128
Task: PPIVOL_D
PRF: 1014Hz
Elevation:1.5
Max Range:128 km
17:13:30
9 OCT 2023 HKT
Corr Velocity in m/s
C
D

(b)

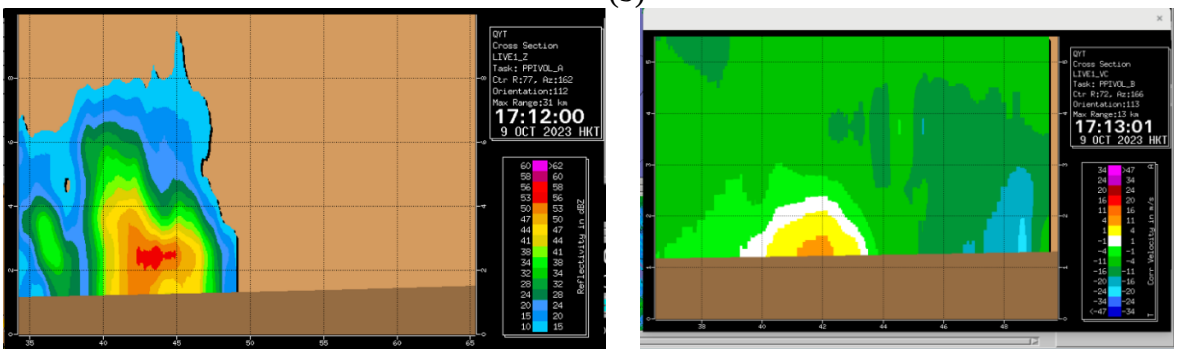
17:12:00
9 OCT 2023 HKT
17:13:01
9 OCT 2023 HKT

(c)

Figure 18. (a) Reflectivity and (b) radial velocity based on 1.5 ° PPI scan of the QYTWR at around 09:13 UTC on 9 October 2023. An intense radar echo displaying comma shape (red ellipse) was observed over the seas to the west of the Dangan islands in (a); while a velocity couplet (red ellipse) was observed in (b) in association with the comma shape intense echo in (a). (c) Cross-section along the A-B plane in (a) showing the maximum reflectivity core located at height of around 2.5 km (left panel); while the cross-section along the C-D plane in (b) showing the maximum velocity of the waterspout reaching above 20 m/s with height around 2 km (right panel).

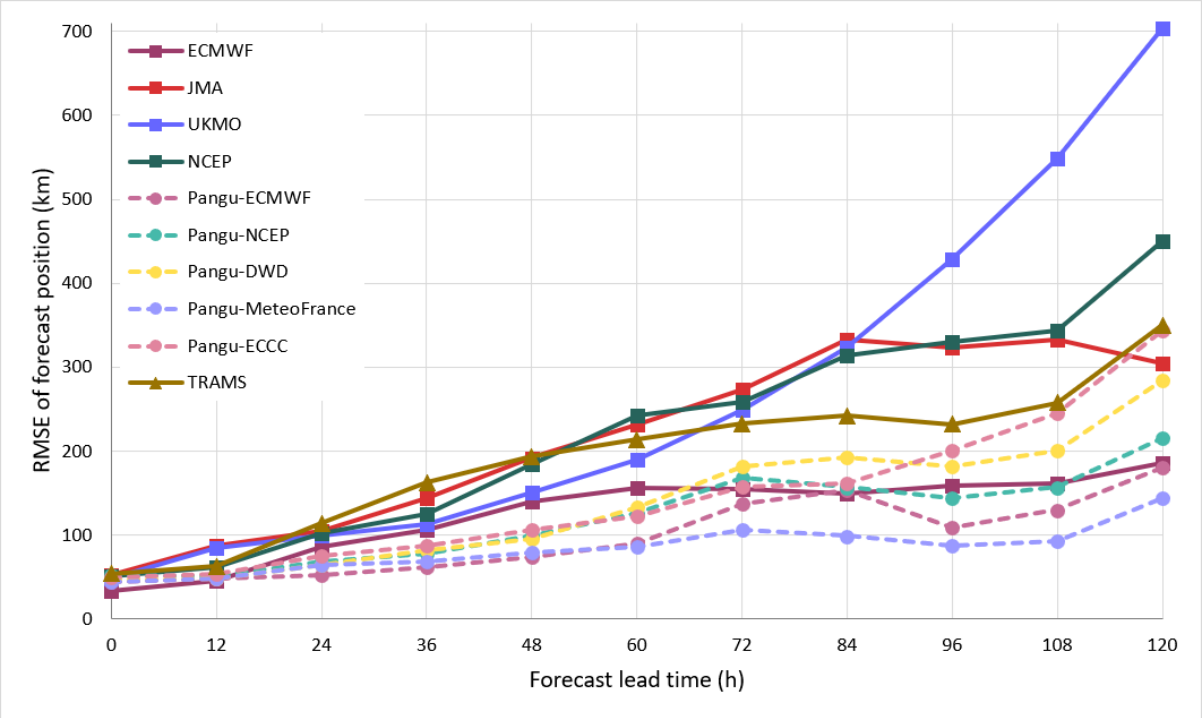

Figure 19. Root-mean-square error of model forecast positions of Koinu as a function of forecast hours. Forecasts are verified against Koinu's analysis positions based on HKO's operational warning track, and homogenized to have a common data set among different models. Dashed lines are verification results of forecasts from Pangu-Weather initialized respectively with the operational analyses of DWD, ECCC, ECMWF, MeteoFrance and NCEP models.